

Miscibility Matrices Explain the Behavior of Grayscale Textures Generated by Gibbs Random Fields

I. M. Elfadel* R. W. Picard†
Massachusetts Institute of Technology
Cambridge, MA 02139

Abstract

This paper describes an original approach to the analysis and prediction of graylevel textures generated as equilibrium states of Gibbs/Markov random fields. This approach is physically motivated by the analogy that exists between the graylevel textures and the miscibility patterns of multiphase flows. The physics of the situation is captured using miscibility matrices that are related to the co-occurrence matrices classically used for texture discrimination. Simulations are provided to motivate and illustrate our approach.

1 Introduction

This paper describes an original approach to the analysis and prediction of graylevel textures generated as equilibrium states of Gibbs/Markov (MRF) random fields. This approach is physically motivated by the analogy that exists between the graylevel textures and the miscibility patterns of multiphase flows. The physics of the situation is captured using miscibility matrices that are related to the co-occurrence matrices classically used for texture discrimination. The approach described in this paper provides a direct link between the MRF methods for texture synthesis and the statistical methods such as co-occurrence matrices. The miscibility matrices also reveal large scale structure that is not revealed by the MRF bonding parameters.

The paper is organized as follows. In Section 2 we briefly review the fundamentals of texture synthesis using MRF models. In Section 3 the new concepts of aura, aura measures, and miscibility matrices are introduced. These are then applied in Section 4 to give a miscibility formulation to the MRF texture synthesis method. Simulations supporting the miscibility approach to MRF texture synthesis are given in Section 5.

2 The MRF Approach to Texture Synthesis

2.1 Background

One-dimensional and causal Markov models have a long history of usefulness for many image processing applications. Since the establishment of the equivalence between Gibbs and Markov random fields, there has been renewed

emphasis on 2-D noncausal MRF's. In particular, these MRF's have been explored for the representation of natural texture patterns [1, 2, 3, 4]. The assumption that the MRF can model image textures has also been used to justify MRF models in image restoration, compression, segmentation, and classification [5, 6, 7, 8].

We model the image as a finite rectangular lattice \mathcal{S} with a neighborhood structure $\mathbf{N} = \{\mathcal{N}_s, s \in \mathcal{S}\}$, where $\mathcal{N}_s \subseteq \mathcal{S}$ is the set of neighbors of the site $s \in \mathcal{S}$. Every site $s \in \mathcal{S}$ will be assigned an integer $x_s \in \Lambda = \{0, 1, \dots, n-1\}$ representing the graylevel value of the pixel at site s . We denote by \mathbf{x} the vector $(x_s, 1 \leq s \leq |\mathcal{S}|)$ of site graylevel values and by Ω the set $\Lambda^{|\mathcal{S}|}$ of all values taken by \mathbf{x} . The graylevel sets of the lattice are defined as follows:

$$\mathcal{S}_g = \{s \in \mathcal{S} | x_s = g\}, \forall g \in \Lambda. \quad (1)$$

It is clear that the graylevel sets constitute a partition of the lattice into mutually disjoint subsets.

The neighborhood structure will be assumed symmetric, i.e.,

$$\forall s, r \in \mathcal{S}, \quad s \in \mathcal{N}_r \text{ if and only if } r \in \mathcal{N}_s. \quad (2)$$

This assumption is required for application to a homogeneous Gibbs random field. The MRF model is usually described by its order, which defines its neighborhood configuration. In Figure 1 (a) neighborhoods of orders 1-4 are shown. These are the only orders used in this paper, though extension to higher orders is straightforward.

Throughout this paper we assume toroidal boundary conditions, where the top pixels are identical to those of the bottom and the right pixels to the left ones. This assumption simplifies the neighborhood notation because on the toroidal lattice the neighborhoods at each site \mathcal{N}_s , are the translates of a basic neighborhood \mathcal{N} . In this case, the number of elements, $|\mathcal{N}_s|$, of each neighborhood is constant and equal to $|\mathcal{N}|$. If boundary conditions other than toroidal are made, then care should be taken in defining the neighborhoods of the sites that lie on the lattice boundaries. In particular, the size of the neighborhood will vary along the boundaries and will be different from the size of the inner site neighborhoods.

The basic methodology for MRF texture synthesis is the following. For the finite toroidal lattice \mathcal{S} , with the symmetric neighborhood structure $\{\mathcal{N}_s, s \in \mathcal{S}\}$, we define the Gibbs energy

$$E(\mathbf{x}) = \sum_{s \in \mathcal{S}} V_s(x_s) + \sum_{s \in \mathcal{S}} \sum_{r \in \mathcal{N}_s} V_{sr}(x_s, x_r), \quad (3)$$

where the V_s 's are the single site potentials and the V_{sr} 's

¹Research Laboratory of Electronics

²Media Laboratory

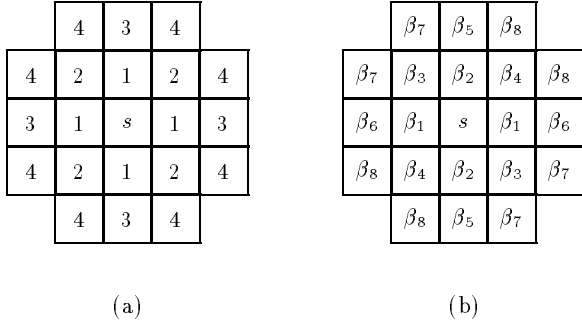


Figure 1: (a) Neighbors of the point s for model orders 1-4. The neighborhood of order p contains all points with labels $\leq p$. (b) The autobinomial parameter for each neighbor.

are the two-site potentials¹, where $V_{sr} = V_{rs}$. In the physics literature, the single-site potentials are called the external field while the two-site potentials define the interaction of the so-called internal field. To the Gibbs energy, thus defined, we can assign a random field whose probability distribution is given by

$$P(\mathbf{x}) = \frac{1}{Z} \exp(-\frac{1}{T}E(\mathbf{x})), \quad (4)$$

where T is the “temperature” of the field and Z is a positive normalizing constant, also known in the physics literature as a partition function. It is not difficult to prove that the above joint probability distribution defines a Markov random field with respect to the neighborhood structure $\{\mathcal{N}_s, s \in \mathcal{S}\}$ [9]. Samples of this MRF correspond to different texture patterns. In this paper we are particularly interested in characterizing the minimum energy patterns, i.e., finding the texture pattern \mathbf{x} that maximizes $P(\mathbf{x})$ in (4). The actual energy minimization procedure is based on a Monte-Carlo algorithm with simulated annealing [5], in which the temperature is gradually lowered according to a schedule slow enough to keep the lattice sites in thermal equilibrium.

2.2 The Autobinomial Model

Different conditional probability distributions can be obtained by specifying the actual expressions of the external and internal potentials. When these conditional probabilities have a binomial distribution, the MRF model is called autobinomial [10]. Besag’s autobinomial model was first used as a model for texture synthesis by Cross and Jain [2], who used the uniform histogram assumption and the Metropolis exchange algorithm to generate texture patterns. The potential functions of the autobinomial model are given by

¹The reader familiar with MRF theory might notice that the double summation in (3) is over all sites and all their neighbors and not over the two-site cliques of the neighborhood structure. We have $V_{sr} = V_{rs} =$ half the two-site clique potential.

$$V_s(x_s) = -\alpha_s x_s - T \ln \binom{n-1}{x_s},$$

$$V_{sr}(x_s, x_r) = -\beta_{sr} x_s x_r,$$

where α_s, β_{sr} are real numbers and $\binom{n-1}{x_s}$ is the binomial coefficient “ $n-1$ choose x_s .”

The corresponding Markov conditional probability distributions (local characteristics) are binomial and given by

$$P(x_s | x_r, r \in \mathcal{N}_s) = \binom{n-1}{x_s} \theta_s^{x_s} (1-\theta_s)^{n-x_s-1},$$

where

$$\theta_s = e^{\tau_s} / (1 + e^{\tau_s}),$$

$$\tau_s = \frac{1}{T} \left(\alpha_s + \sum_{r \in \mathcal{N}_s} \beta_{sr} x_r \right).$$

In the homogeneous case $\alpha_s = \alpha$ (site-independent), and $\beta_{sr} = \beta_r$ (site-independent but possibly dependent on the direction of the neighbor). In Figure 1 (b) the autobinomial “bonding parameter” which multiplies each neighbor is shown. The autobinomial parameters are *isotropic* when $\beta_r = \beta, \forall r \in \mathcal{N}$. When the model is first order isotropic and $n = 2$, we get a binary nearest-neighbor model from which the famous Ising model [11] can be derived by making the transformation $x_s \rightarrow 2x_s - 1$.

2.3 The Metropolis Exchange Algorithm

In this paper, we follow [2] in using the Metropolis exchange algorithm as our Monte-Carlo algorithm. The exchange algorithm enforces a uniform histogram constraint that prevents trivial solutions for the minimum energy configuration.

In the exchange algorithm, two different lattice sites are picked up randomly and their pixel values, if different, are exchanged. The energy change due to the exchange is computed and used in a Metropolis decision rule² [5] for lattice state update. The ingenuity of this rule is that it completely eliminates the need for computing the partition function Z – a usually burdensome task. When the external field in (3) is homogeneous, i.e., the V_s ’s are independent of the site location s , it has no influence on the site update. This is because it cancels out from the expression of the energy change. Thus, we omit the homogeneous external field terms from the Gibbs energy. It follows that the problem of texture synthesis using a Markov random field model in conjunction with a uniform histogram constraint can be formulated as the following constrained integer nonlinear programming problem:

$$\min_{\mathbf{x} \in \Omega} \sum_{s \in \mathcal{S}} \sum_{r \in \mathcal{N}_s} V_{sr}(x_s, x_r), \quad (5)$$

$$\text{subject to } |\mathcal{S}_g| = \gamma, \forall g \in \Lambda.$$

²Sites are updated with probability $\min(1, \exp(-\Delta E/T))$, where ΔE is the energy change.

It is important to stress that the constraints of this problem are implicitly satisfied when an exchange algorithm is used. Thus, in all the texture synthesis examples of this paper where we start with an initial histogram satisfying $|\mathcal{S}_g| = \gamma, \forall g \in \Lambda$, these constraints will also be satisfied by the final pattern. When a non-exchange method is used, these constraints can be easily incorporated into the objective function via a penalty function.

When the autobinomial model is synthesized using the Metropolis exchange algorithm, it has the property of symmetry with respect to the graylevel values. That is, if we have graylevels $g \in \Lambda = \{0, 1, \dots, n-1\}$, then if we replace all the graylevels according to $g \rightarrow n-1-g$, the parameters of the synthesized pattern do not change. We will find this useful in simulations when we analyze the patterns formed.

It is important to note that the texture patterns produced in studies such as Cross and Jain’s [2] are at non-equilibrium. Equilibrium is defined as the minimum energy state, that is, the state which maximizes the exponent in the Gibbs joint probability. Monte-Carlo texture synthesis methods produce many non-equilibrium states on the way to equilibrium. Many of these non-equilibrium states look like natural textures. One of the shortcomings of the MRF approach to date is that it has been difficult to predict the evolution of the texture patterns during the equilibrating process.

3 Auras, Aura Measures, Miscibility Matrices

3.1 Auras

We now introduce a novel set-theoretic concept that gives a precise mathematical meaning to the notion of how one set B is present in the neighborhood of some other set A .

Definition 1 *Let A, B be two subsets $\subseteq \mathcal{S}$. Then the aura of A with respect to B for the neighborhood structure $\mathbf{N} = \{\mathcal{N}_s, s \in \mathcal{S}\}$ is a subset of \mathcal{S} defined by*

$$\bigcup_{s \in A} (\mathcal{N}_s \cap B). \quad (6)$$

The aura of a set A with respect to a set B will be denoted by

$$\mathcal{O}_B(A, \mathbf{N}). \quad (7)$$

The aura of a set with respect to itself will be called the self-aura.

This definition remains valid even if the neighborhood structure is not symmetric. Note that the sets A and B are not necessarily graylevel sets. They in fact could be any sets of labels whose interaction we would like to study. However, in the context of grayscale texture generation, we will deal essentially with the auras of graylevel sets.

It is very important to note that the aura depends on the neighborhood structure chosen for the lattice. All the results derived in this paper are valid for any choice of the \mathcal{N}_s ’s, including non-nearest neighbors. In all the derivations, the structure \mathbf{N} is assumed to be given once and for all. Thus, we choose to omit the notational dependency on \mathbf{N} from (7) and use for the aura the simplified

notation $\mathcal{O}_B(A)$. Note that in general, $\mathcal{O}_B(A) \neq \mathcal{O}_A(B)$, and that $A \not\subseteq \mathcal{O}_A(A)$, unless every site belongs to its own neighborhood³.

The aura has a number of other properties that can be derived using its definition and elementary set operations. The reader is referred to [12] for a list of the most important of these properties. In particular, it can be shown [12] that the aura can be computed using morphological operations [13].

The choice of the word “aura” was motivated by the situation that arises when we look at $\mathcal{O}_{A^c}(A)$, that is, the neighbors of the sites of A that are in the complementary set of A . When the neighborhood of A is noncausal and has nearest neighbors, as in the case of MRF’s, the aura set forms a ring around A .

3.2 Aura Measures

In addition to the idea of the presence of one set B in the neighborhood of another set A , we need a measure of how *much* of B is present in A . The easiest way for measuring the size of the aura of a set A with respect to a set B is by counting the number of elements, $|\mathcal{O}_B(A)|$. Note that we have, from the definition and from the known properties of sets

$$|\mathcal{O}_B(A)| \leq \sum_{s \in A} |\mathcal{N}_s \cap B|. \quad (8)$$

In problems involving image synthesis or processing, it is the right side that appears more frequently. In particular, we will see in Section 3.3 and Section 4.4 that the right side relates closely to image co-occurrence statistics [14]. It also turns out that the right side is a better measure of how “broken” the boundary of the set A is. For these reasons, the following definition of the measure of an aura is adopted:

Definition 2 *Let A, B be two subsets $\subseteq \mathcal{S}$. Then the aura measure, denoted by $m(A, B)$, is defined by*

$$m(A, B) = \sum_{s \in A} |\mathcal{N}_s \cap B|. \quad (9)$$

When A and B are two graylevel sets S_g and $S_{g'}$, the aura measure will be denoted $m(g, g')$. Since the neighborhood structure is assumed symmetric we have $m(A, B) = m(B, A)$ and for graylevel sets $m(g, g') = m(g', g)$ [12]. The aura measure has an intuitive interpretation as the amount of mixing between the sets A and B . A large aura measure means the two sets try to mix with each other; a small aura measure means they try to separate. The aura measure of A with respect to its complementary set A^c can be understood as a measure of the boundary length of A . This measure is compatible with the scale at which we look at the image. This scale is expressed by the neighborhood shape and size. Also, from a graph-theoretical point of view, the aura measure is a generalization of the concept of an edge boundary for a subgraph [15].

When there is an exchange operation between A and B , as in the Metropolis exchange algorithm, the self-aura measure of $A \cup B$ remains constant, which puts a constraint

³This situation is not allowed in the context of MRF image models.

on the self-aura and aura measures of A and B before and after the exchange.

Other details on the properties of the aura measure are provided in [12].

3.3 Miscibility Matrices

Before applying the above concepts to texture synthesis using MRF's, we introduce a useful tool, based on the intuitive understanding of the aura measure as a miscibility/immiscibility measure, the *miscibility matrix*. Even though the following definition is valid for any partition of the lattice, it is only given for the grayscale partition.

Definition 3 Let $S_g \subseteq \mathcal{S}$, $\forall g \in \Lambda$, be the graylevel sets of the image. Then the miscibility matrix, \mathbf{M} , is the $n \times n$ integer matrix defined by $\mathbf{M} = [m(g, g')]$, $\forall g, g' \in \Lambda$.

The following proposition whose proof appears in [12] contains some of the properties of the miscibility matrix.

Proposition 4 (Miscibility Matrix Properties) Let \mathbf{M} be a miscibility matrix. Then,

(a) Each row sum satisfies:

$$\sum_{g'=0}^{n-1} m(g, g') = |S_g| |\mathcal{N}|, \forall g \in \Lambda;$$

(b) Each column sum satisfies:

$$\sum_{g=0}^{n-1} m(g, g') = |S_{g'}| |\mathcal{N}|, \forall g' \in \Lambda;$$

(c) If \mathcal{N} is symmetric, then \mathbf{M} is symmetric, and

$$\sum_{g=0}^{n-1} m(k, g) = \sum_{g=0}^{n-1} m(g, k) = |S_k| |\mathcal{N}|, \forall k \in \Lambda.$$

When the neighborhood contains only one element the miscibility matrix becomes identical to a pairwise co-occurrence matrix [14]. If the neighborhood contains a pair of symmetric neighbors, the miscibility matrix is a symmetric co-occurrence matrix. The general relationship between miscibility and co-occurrence matrices will be seen in Section 4.4.

Under a uniform histogram constraint the miscibility matrix can be normalized by $\gamma |\mathcal{N}|$ to become a doubly stochastic matrix that can be interpreted as a statistical estimate of a probability co-occurrence matrix. Relating the miscibility matrix to the parameters of the MRF model from which the texture was obtained can be done for the binary, homogeneous, isotropic case (the Ising model) [16].

4 Reformulation of MRF Using Miscibility

In this section, we rewrite the energy function of the Gibbs distribution in terms of aura measures. The aura formulation re-interprets the energy function as an interaction between miscibilities. With this intuitive interpretation, one can ask questions such as “are colors A and

B maximally separated yet?” The answers to these questions characterize the pattern's progress toward equilibrium. Thus, the aura measure is a tool for predicting the appearance and arrival of equilibrium states. Some examples of this type of usage will be shown in Section 5.

4.1 Isotropic Field Case

The problem of texture synthesis using an autobinomial Markov random field model in conjunction with the Metropolis exchange algorithm can be formulated, using (5), as the following constrained integer nonlinear programming problem:

$$\begin{aligned} \max_{\mathbf{x} \in \Omega} \quad & \sum_{s \in \mathcal{S}} \sum_{r \in \mathcal{N}_s} \beta_{sr} x_s x_r, \\ \text{subject to} \quad & |\mathcal{S}_g| = \gamma, \forall g \in \Lambda, \end{aligned} \quad (10)$$

where the β_{sr} 's represent the bonds between a graylevel value x_s and its neighbors $x_r, r \in \mathcal{N}_s$. The image field is assumed homogeneous and isotropic so that $\beta_{sr} = \beta$. Then the above optimization problem becomes

$$\begin{aligned} \max_{\mathbf{x} \in \Omega} \quad & \left(\beta \sum_{s \in \mathcal{S}} \sum_{r \in \mathcal{N}_s} x_s x_r \right), \\ \text{subject to} \quad & |\mathcal{S}_g| = \gamma, \forall g \in \Lambda. \end{aligned} \quad (11)$$

The constraints of (11) are not independent because the sum of $|\mathcal{S}_g|$'s, $n\gamma$, must equal $|\mathcal{S}|$. Using the fact that $\{\mathcal{S}_g, g \in \Lambda\}$ is a partition of \mathcal{S} and that when $s \in \mathcal{S}_g, x_s = g$, the above cost function becomes

$$\beta \sum_{g \in \Lambda} g \sum_{s \in \mathcal{S}_g} \sum_{r \in \mathcal{N}_s} x_r. \quad (12)$$

Furthermore,

$$\mathcal{N}_s = \bigcup_{g' \in \Lambda} (\mathcal{N}_s \cap \mathcal{S}_{g'}),$$

and $x_r = g'$, when $r \in \mathcal{S}_{g'}$. It follows that (12) can be written as

$$\beta \sum_{g \in \Lambda} g \sum_{s \in \mathcal{S}_g} \sum_{g' \in \Lambda} \sum_{r \in \mathcal{N}_s \cap \mathcal{S}_{g'}} g' \quad (13)$$

or

$$\beta \sum_{g, g' \in \Lambda} gg' \sum_{s \in \mathcal{S}_g} |\mathcal{N}_s \cap \mathcal{S}_{g'}|. \quad (14)$$

Using the definition of the measure of an aura, we get

$$\beta \sum_{g, g' \in \Lambda} gg' m(g, g'). \quad (15)$$

Thus the problem of MRF texture generation in the grayscale domain has been transformed to an optimization problem with a linear cost function in the “miscibility domain.” Note that the above derivation can be repeated for *any* homogeneous, isotropic, internal interaction field $V_{sr} = V$ between graylevels. For this general case we get the following constrained minimization problem

$$\begin{aligned} \min_{\mathbf{x} \in \Omega} \quad & \left(\sum_{g \in \Lambda} V(g, g) m(g, g) + 2 \sum_{g < g'} V(g, g') m(g, g') \right), \\ \text{subject to} \quad & |\mathcal{S}_g| = \gamma, \forall g \in \Lambda. \end{aligned}$$

A special case worth noting is the homogeneous isotropic Potts model [17], for which

$$V(g, g') = 2\delta_{gg'} - 1,$$

where $\delta_{gg'}$ is the Kronecker δ symbol. The Ising model is also a special case of the Potts model.

For the autobinomial case, the resulting patterns depend strongly on *both* the sign of β and the number of graylevels. The simulations of Section 5 show that the miscibility framework is very appropriate for the explanation and prediction of these patterns.

4.2 Constraints on Miscibilities

From an optimization point of view, the most interesting fact about expressing the cost function in terms of the aura measures is that it becomes linear as a function of these variables. We can go one step further along the way of transforming the nonlinear integer programming problem into a linear problem by introducing linear constraints on the aura measures. These linear constraints are of two kinds: equality constraints due to the uniform histogram assumption and inequality constraints imposed by the lattice geometry and the boundary conditions. The first kind of constraints can be readily obtained from Proposition 4. Note that because of the symmetric neighborhood assumption, equation (c) of Proposition 4 is satisfied. Therefore the aura measures satisfy $n = |\Lambda|$ equality constraints given by

$$\sum_{g' \in \Lambda} m(g, g') = |\mathcal{S}_g| |\mathcal{N}|, \forall g \in \Lambda. \quad (16)$$

The inequality constraints are more difficult to obtain, because they strongly depend on the particular texture synthesis problem we are dealing with. To give the reader a flavor of these constraints, let us consider the binary ferromagnetic Ising model ⁴ with uniform histogram and toroidal boundary conditions. Defining the graylevel sets \mathcal{S}_0 (black pixels) and \mathcal{S}_1 (white pixels) the cost function to be minimized is reduced to $-m(1, 1)$ under the constraints

$$\begin{aligned} m(0, 0) + m(0, 1) &= 2|\mathcal{S}|, \\ m(0, 1) + m(1, 1) &= 2|\mathcal{S}|. \end{aligned}$$

Minimizing the cost function means maximizing the clumpiness of the white pixels, which also means, because of the uniform histogram constraint, maximizing the clumpiness of the black pixels. It follows from the above linear constraint that the boundary between the two graylevel sets as expressed by the aura measure $m(0, 1)$ is minimized. It is clear that the simultaneous presence of both black and white pixels imposes a lower bound on $m(0, 1)$. This lower bound depends on the geometry of the lattice. For a square toroidal lattice, $|\mathcal{S}| = N^2$, the lower bound is $2N$ and is reached by a configuration in which the black and white pixels form two stripes adjacent to each other. When the lattice is rectangular these two stripes will be parallel to the smaller of the rectangle dimensions. The reader is referred to Section 5 for examples of equilibrium patterns on non-square lattices.

⁴In this example the binary state is taken to be 0 or 1.

If we now define the vectors

$$\begin{aligned} \mathbf{m} &= (m(0, 0), m(0, 1), \dots, m(0, n-1), \\ &\quad m(1, 0), \dots, m(n-1, n-1))^T, \\ \mathbf{V} &= (V(0, 0), V(0, 1), \dots, V(0, n-1), \\ &\quad V(1, 0), \dots, V(n-1, n-1))^T, \end{aligned}$$

where $V(g, g') = gg'$, then the constrained *nonlinear* integer program can be reformulated as the following constrained *linear* integer program

$$\min_{\mathbf{m} \geq 0} \mathbf{V}^T \mathbf{m}$$

$$\text{subject to } \mathbf{Bm} = \mathbf{b}, \mathbf{Dm} \geq \mathbf{d}.$$

In principle, it is possible to solve this problem directly in the miscibility domain. In many cases the inequality constraints can be derived from a simple analysis of the lattice geometry and histogram constraints [12].

4.3 Boundary Optimization Principle

4.3.1 Ising Model

As mentioned, the Ising model is a special case of both the autobinomial and Potts models. Let S_1 be the set of sites with spin up, and S_{-1} be the set of sites with spin down. The optimization problem, as a special case of the Potts model optimization, becomes

$$\min_{\mathbf{x} \in \Omega} (-\beta)[m(S_{-1}, S_{-1}) + m(S_1, S_1) - 2m(S_1, S_{-1})].$$

Note that we have omitted the histogram constraint for this example. When $\beta > 0$, the expression between brackets is maximized. The maximum occurs when either every site is 1 or every site is -1 so that $m(S_{-1}, S_1) = 0$ (spontaneous magnetization). This means that the boundary between the two regions is minimized; actually, its length is zero here. When $\beta < 0$, the expression is minimized. This corresponds to the antiferromagnetic phase. In general the energy optimization problem can be recast as a boundary optimization problem. Similar conclusions hold under the uniform histogram constraint. For the Ising model on a lattice of known size, if we know the total number of up spins $|S_1|$ and the total number of pairs of up spins $m(S_1, S_1)$, the model is completely characterized. This characterization in terms of boundary length, well known in the physics literature [11], is a special case of Proposition 4.

4.3.2 The General Case

The above conclusions about the boundary optimization principle in the binary case can be easily generalized to an arbitrary number of graylevels and an arbitrary neighborhood order. For instance, without any histogram constraint, the patterns generated by the isotropic autobinomial model with positive β will become all white. This can be interpreted as a trivial boundary minimization, where the boundary lengths are all zero. When a uniform histogram is imposed on the patterns, the situation is slightly more complicated, but can still be understood in terms of mixing (boundary maximization) and separation (boundary minimization). Simulations are provided in Section 5 that show boundary optimization properties of the autobinomial model in the graylevel case.

4.4 Anisotropic Field Case

The objective of this section is to extend the definition of the aura and of the miscibility matrix to accommodate the important cases where anisotropic field phenomena need to be taken into account. This is typically the case with textures synthesized through anisotropic Gibbs random fields. In order to capture the influence due to directionality, we will assume that the neighborhood of each site can be partitioned into K subneighborhoods, so that in each subneighborhood the field behaves isotropically. More formally, we will write

$$\mathcal{N}_s = \bigcup_{k=1}^K \mathcal{N}_s^k, \quad \forall s \in \mathcal{S}, \quad (17)$$

where $\mathcal{N}_s^k \cap \mathcal{N}_s^l = \emptyset$, unless $l = k$. Then we can define the aura of the subset A with respect to the subset B for the k -th subneighborhood structure by

$$\mathcal{O}_B^k(A) = \bigcup_{s \in A} (B \cap \mathcal{N}_s^k). \quad (18)$$

It can be readily seen using the above definition that

$$\mathcal{O}_B(A) = \bigcup_{k=1}^K \mathcal{O}_B^k(A). \quad (19)$$

If each subneighborhood has size 1, then the measures of $\mathcal{O}_B^k(A)$ are co-occurrences. Let $m^k(A, B)$ be the measure of $\mathcal{O}_B^k(A)$. We have

$$m(A, B) = \sum_{k=1}^K m^k(A, B), \quad (20)$$

so that the aura measures are a linear combination of co-occurrences.

Specifically, for the autobinomial model, if the β_k 's are anisotropic, the equilibrium solution will be achieved by solving

$$\begin{aligned} \max_{\mathbf{x} \in \Omega} & \left(\sum_{g, g' \in \Lambda} gg' \sum_{k=1}^K \beta_k m^k(g, g') \right), \\ \text{subject to} & \quad |\mathcal{S}_g| = \gamma, \quad \forall g \in \Lambda. \end{aligned} \quad (21)$$

The simulations given in the next section support the intuition that can be derived from the anisotropic miscibility analysis of the above linear programming problem.

5 Simulations

5.1 Mixing and Separation

As mentioned, the patterns produced by the MRF texture model in the extensive study by Cross and Jain [2] were non-equilibrium patterns. In this paper, we apply the aura measures to the analysis of MRF patterns near equilibrium. The simulations here assume toroidal boundary conditions and the autobinomial MRF energy function described in Section 2.

The samples have been synthesized by the Metropolis exchange method, with log annealing according to

$$T = \frac{c}{\log(p+1)},$$

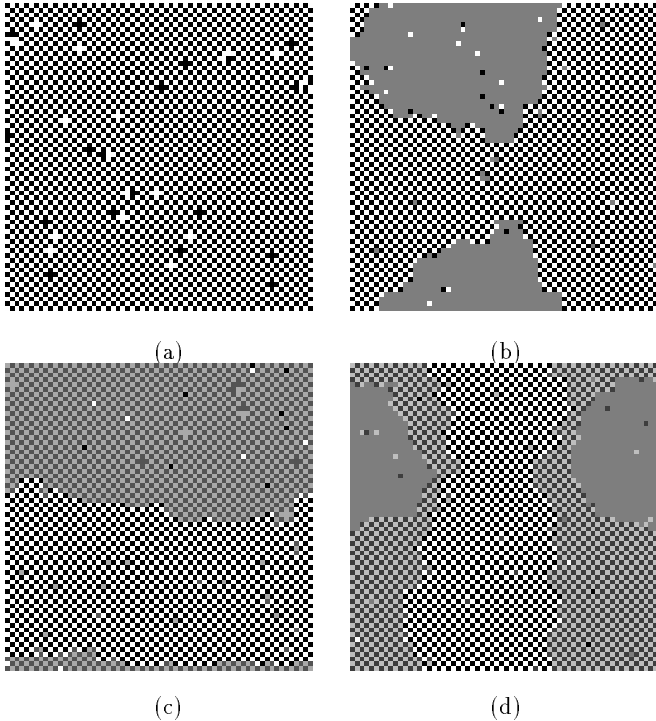


Figure 2: Examples of near-equilibrium patterns for first-order MRF's with negative isotropic parameters. Images (a)-(d) correspond to 2-5 graylevels respectively. Each image is 64×64 .

where $p = \lfloor k/10 \rfloor$ and $k = 0, 1, \dots$ is the iteration number. The scale factor in the numerator is typically chosen in the range $c \in (0, 10]$. In our simulations, $c = 1$. Though its choice is ad hoc, its behavior is understood as a rate constant that is proportional to how slow the annealing progresses. One iteration is counted as N^2 attempted exchanges. An exchange is attempted whenever two randomly picked sites have different locations and graylevels. The total number of iterations for the patterns was 10000, with the temperature lowered according to the above schedule every 10 iterations. The initial state for all these simulations was a random noise image with uniform histogram. Because of the exchange operation, the histogram is preserved throughout the texture synthesis, and the (assumed constant) external field can be ignored.

For isotropic parameters, the behavior of the autobinomial MRF is well described by its graylevel miscibilities. In Figure 2 are shown four texture samples corresponding to first-order negative isotropic parameters. All of these have identical parameters; the only difference is that the number of graylevels in (a)-(d) changes from 2-5. These patterns are close enough to equilibrium that the minimum energy characteristics are easily seen. In (a) we see the checkerboard being made in an effort to minimize $m(1, 1)$ (white self-miscibility). The terms $m(0, 0)$ and $m(0, 1)$ are multiplied by zero and can be ignored. Optimization is achieved by moving blacks between all the whites, so that the miscibility of the whites goes to zero. In (b) the sum of $m(1, 1)$,

$4m(2,2)$, and $4m(1,2)$ is minimized. The last two terms have the greatest weight, and can be interpreted as color 2 (white) trying to form a checkerboard, but not with color 1 (gray). This leaves the configuration of a checkerboard between colors 0 (black) and 2, with color 1 forming a blob off by itself. To minimize the term $m(1,1)$, it would be necessary to have a fourth color to mix with it. This happens in (c). The image in (d) and images made with higher numbers of graylevels have similar explanations, all deriving from intuition about mixing.

For positive isotropic parameters, the behavior is described by immiscibility, the separation of the different colors. Figure 3 is identical to that of Figure 2 with the exception of the sign of β . In (a) we see separation of black and white as $m(1,1)$ is maximized. As white mixes only with white, black is forced to mix only with black. If the synthesis of this energy function were done using a non-exchange method such as the Gibbs Sampler, the optimal pattern would be solid white. The black remains only because of the exchange method, which preserves the histogram of the lattice. In (b) the sum of $m(1,1)$, $4m(2,2)$, and $4m(1,2)$ is maximized. Graylevel 2 forms a blob while maximizing the presence of graylevel 1 along its boundary. Graylevel 0 has no other choice but to form a blob. The image in (c) and images made with higher numbers of graylevels have similar explanations which derive from intuition about separation.

As mentioned before, for autobinomial fields synthesized with the Metropolis exchange, the result should be the same if all the graylevels of value g are replaced with those of value $n - g - 1$. This graylevel symmetry shows up in the miscibility behavior. For example, both black (0) and white ($n - 1$) have the same mixing behavior in all the samples shown in this section.

5.2 Boundary Maximization and Minimization

The mixing and separation described in the previous section has another interpretation in terms of the principle of graylevel boundary length. The behavior that was described for the Ising model in Section 4.3.1 is an example of the boundary length optimization for the binary case. The examples in Figure 2 are also examples of maximizing graylevel boundary length for a general number of graylevels. Similarly, Figure 3 gives examples of minimizing graylevel boundary length.

When the lattice geometry is not square, the boundary minimization manifests itself in a slightly different way. As mentioned in Section 4.2, there is a geometry-dependent lower bound for the cross-miscibility measures. Of all the configurations that separate white and black, the one they will choose will be the one with minimum total boundary length. On a 32×64 lattice, this is a left-right separation, with boundary length proportional to 2×32 . (There are two boundaries since the lattice is toroidal). An example of this selection is illustrated in Figure 4 for graylevels 2 and 3. The parameters used to synthesize these patterns are identical to those used in Figure 3 (a) and (b), but the model order has been increased to fourth. The higher order neighborhood is responsible for the less noisy appearance of these patterns.

5.3 Miscibility Matrices and Isotropic Texture Samples

The notions of boundary length and miscibility are numerically stated by the miscibility matrices. These matrices for the texture samples of Figure 2 (a)-(d) are shown in Figure 5. Note that the auras were all formed with first order neighborhoods ($|\mathcal{N}| = 4$), as the texture samples are all first order MRF's. The properties of Proposition 4 are easily checked for the $|\mathcal{S}| = 64 \times 64$ lattices used here. We note that all of the aura matrices are becoming anti-tridiagonal. For the positive bonding parameters, they become tridiagonal. These are shown in Figure 6. The diagonal dominance of co-occurrence matrices has long been understood to relate to texture clumpiness [18]. Here we have a precise formulation of clumpiness as the aura self-measures.

We have begun investigating the ability of the aura to measure the distance away from equilibrium of a texture pattern. For positive isotropic textures, we know that the miscibility matrix will become tridiagonal. The lattice geometry constrains the sup-diagonal terms, which when coupled with Proposition 4, leaves us with a known optimal value for the trace of the matrix. Thus, a measure of the trace of the miscibility matrix gives an estimate of texture pattern convergence. The traces of the normalized aura matrices for seven near-equilibrium patterns such as those shown in Figure 3 were plotted. The result is a straight line, indicating that the trace grows linearly with the number of graylevels for positive isotropic patterns. For higher order neighborhoods, the matrices tend toward diagonal even faster, resulting in a steeper slope of the trace vs. graylevel line. Similar opposite behavior occurs for negative parameters and anti-traces.

5.4 Anisotropic Fields

The samples shown thus far are all synthesized with isotropic parameters. As the relative weights of the parameters are changed, the relative weights of the miscibilities change as given in (21). In Figure 7, the parameters are $\beta_1 = 1$ (horizontal), $\beta_2 = 1$ (vertical) on the left, and $\beta_1 = 1$, $\beta_2 = 2$ on the right. The stronger vertical clustering is apparent on the right. Similarly, Figure 8 has parameters $\beta_1 = -1$, $\beta_2 = -1$ on the left, and $\beta_1 = -1$, $\beta_2 = -2$ on the right. Here, the vertical tug is evident from the vertical crystal defects. These result because the repulsion between vertical pairs is stronger than the repulsion between horizontal pairs.

6 Summary

In this paper, a systematic approach for analyzing and predicting the equilibrium patterns of textures generated by MRF models has been introduced. The approach is based on a set-theoretic concept, the aura of one set with respect to another, and on a physically motivated framework, boundary length and miscibility in multiphase fluids. Based on the aura/miscibility framework and the simulations, we can make the following conclusions:

- . A new set-theoretic concept, the "aura", has been introduced and shown to provide a coherent new explanation of the behavior of MRF texture patterns.
- . The new aura framework allows the rewriting of the nonlinear MRF energy function as a linear combina-

tion of aura measures.

The aura measure has a miscibility interpretation which allows the texture patterns to be both mathematically and intuitively characterized by the amount of mixing and separation between graylevels.

The miscibility matrix, formed from the aura measures, is shown to be related to the classical co-occurrence matrix. The miscibility matrix thus links the popular co-occurrence analysis tool to MRF's.

The miscibility optimization, which holds for any number of graylevels, generalizes the boundary length optimization property of the binary Ising model.

During the synthesis of texture the lattice geometry and Metropolis exchange algorithm enforce constraints on the miscibility matrix. These constraints allow the miscibility matrix to be a useful tool for measuring distance from equilibrium.

The miscibility matrix also contains information about global interactions between graylevel sets. These global interactions result in a large scale structure that cannot be inferred from the MRF bonding parameters alone.

Even though we are still in the process of exploring the aura/miscibility framework for texture analysis and prediction, we feel that the work presented in this paper has already confirmed Besag's observation that we quote from his seminal paper [10]:

Incidentally, the fact that a scheme is formally described as "locally interactive" does not imply that the patterns it produces are local in nature (cf. the extreme case of long-range order in the Ising model).

7 Acknowledgments

The authors acknowledge the helpful support and encouragement of Prof. John Wyatt, Jr., and Prof. Alex P. Pentland. The work described in this paper was supported by the National Science Foundation and the Defense Advanced Research Projects Agency (DARPA) under Grant No. MIP-88-14612, the National Science Foundation under Grant No. IRI-8719920, the Rome Air Development Center (RADC) of the Air Force System Command and the Defense Advanced Research Projects Agency (DARPA) under contract No. F30602-89-C-0022.

References

- [1] M. Hassner and J. Sklansky. The use of Markov random fields as models of texture. *Comp. Graph. and Img. Proc.*, 12:357-370, 1980.
- [2] G. R. Cross and A. K. Jain. Markov random field texture models. *IEEE T. Patt. Analy. and Mach. Intell.*, PAMI-5(1):25-39, 1983.
- [3] R. Chellappa and S. Chatterjee. Classification of textures using Markov random field models. In *Proc. ICASSP*, pages 32.9.1-32.9.4, San Diego, 1984.
- [4] L. Garand and J. A. Weinman. A structural-stochastic model for the analysis and synthesis of cloud images. *J. of Climate and Appl. Meteorology*, 25:1052-1068, 1986.
- [5] S. Geman and D. Geman. Stochastic relaxation, Gibbs distributions, and the Bayesian restoration of images. *IEEE T. Patt. Analy. and Mach. Intell.*, PAMI-6(6):721-741, 1984.
- [6] H. Derin, H. Elliott, R. Cristi, and D. Geman. Bayes smoothing algorithms for segmentation of binary images modeled by Markov random fields. *IEEE T. Patt. Analy. and Mach. Intell.*, PAMI-6(6):707-720, 1984.
- [7] R. Chellappa. "Two-Dimensional Discrete Gaussian MARKov Random Field Models For Image Processing". In L. N. Kanal and A. Rosenfeld, editors, *Progress In Pattern Recognition 2*. Elsevier Science publishers B. V. (North Holland), 1985.
- [8] H. Derin and H. Elliott. Modeling and segmentation of noisy and textured images using Gibbs random fields. *IEEE T. Patt. Analy. and Mach. Intell.*, PAMI-9(1):39-55, 1987.
- [9] R. Kindermann and J. L. Snell. *Markov Random Fields and their Applications*. American Mathematical Society, Providence, Rhode Island, 1980.
- [10] J. Besag. Spatial interaction and the statistical analysis of lattice systems (with discussion). *J. Roy. Stat. Soc., Ser. B*, 36:192-236, 1974.
- [11] K. Huang. *Statistical Mechanics*. Wiley, 1963.
- [12] R. W. Picard. A staggered-dct decreases perceived blockiness. In *Proc. of the Picture Coding Symposium*, pages 15.3.1-15.3.2, Cambridge, Ma, March 1990.
- [13] P. Maragos and R. W. Schafer. Morphological systems for multidimensional signal processing. *Proc. IEEE*, 78(4):690-710, April 1990.
- [14] R. Haralick. Statistical and structural approaches to texture. *Proc. IEEE*, 67:786-804, May 1979.
- [15] B. Bollobas. *Combinatorics*. Cambridge University Press, 1986.
- [16] G. R. Cross. *Markov Random Field Texture Models*. PhD thesis, Michigan State Univ., 1980.
- [17] R. J. Baxter. *Exactly Solved Models In Statistical Mechanics*. Academic Press, Inc., London, 1982.
- [18] A. Rosenfeld and A. C. Kak. *Digital Picture Processing, Volume 2*. Academic Press, Inc., Orlando, 1982.

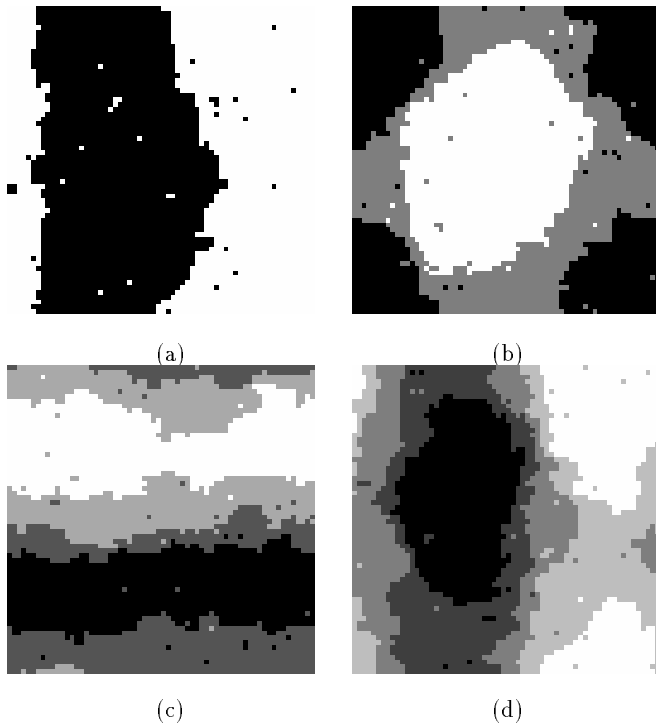
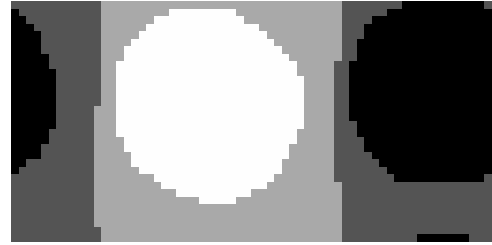


Figure 3: Examples of near-equilibrium patterns for first-order MRF's with positive isotropic parameters. Images (a)-(d) correspond to 2-5 graylevels respectively. Each image is 64×64 .



(a)



(b)

Figure 4: Lattice geometry affects the equilibrium pattern by constraining the miscibilities between different graylevels. In (a), the separation will always make a vertical boundary, since that dimension is the shortest in this 32×64 lattice. Note this pattern is only two exchanges from being at its minimum energy state. Similarly, in (b), the two gray regions try to separate with vertical boundaries.

$$\mathbf{M} = \begin{bmatrix} 138 & 8054 \\ 8054 & 138 \end{bmatrix} \quad \mathbf{M} = \begin{bmatrix} 0 & 170 & 5290 \\ 170 & 5116 & 174 \\ 5290 & 174 & 0 \end{bmatrix}$$

(a)

(b)

$$\mathbf{M} = \begin{bmatrix} 0 & 0 & 159 & 3937 \\ 0 & 34 & 3903 & 159 \\ 159 & 3903 & 34 & 0 \\ 3937 & 159 & 0 & 0 \end{bmatrix}$$

(c)

$$\mathbf{M} = \begin{bmatrix} 0 & 0 & 0 & 140 & 3136 \\ 0 & 0 & 100 & 3032 & 144 \\ 0 & 100 & 3072 & 104 & 0 \\ 140 & 3032 & 104 & 0 & 0 \\ 3136 & 144 & 0 & 0 & 0 \end{bmatrix}$$

(d)

Figure 5: Miscibility matrices corresponding to textures in Figure 2 (a) - (d).

$$\mathbf{M} = \begin{bmatrix} 7878 & 314 \\ 314 & 7878 \end{bmatrix} \quad \mathbf{M} = \begin{bmatrix} 5174 & 286 & 0 \\ 286 & 4904 & 270 \\ 0 & 270 & 5194 \end{bmatrix}$$

(a)

(b)

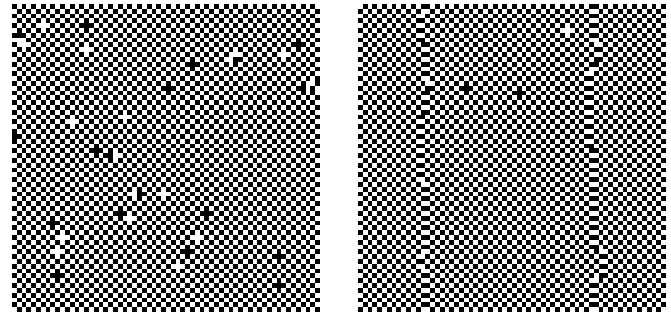
$$\mathbf{M} = \begin{bmatrix} 3850 & 246 & 0 & 0 \\ 246 & 3598 & 252 & 0 \\ 0 & 252 & 3594 & 250 \\ 0 & 0 & 250 & 3846 \end{bmatrix}$$

(c)

$$\mathbf{M} = \begin{bmatrix} 3072 & 204 & 0 & 0 & 0 \\ 204 & 2828 & 244 & 0 & 0 \\ 0 & 244 & 2794 & 238 & 0 \\ 0 & 0 & 238 & 2836 & 202 \\ 0 & 0 & 0 & 202 & 3078 \end{bmatrix}$$

(d)

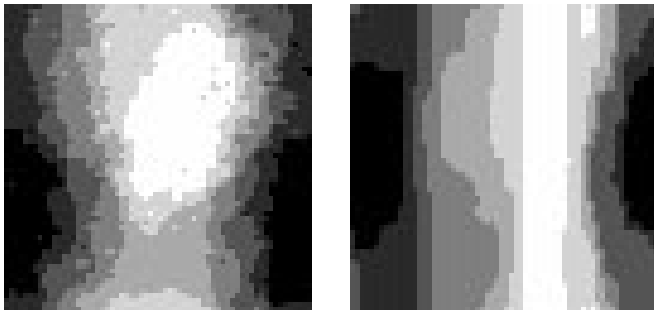
Figure 6: Miscibility matrices corresponding to textures in Figure 3 (a) – (d).



(a)

(b)

Figure 8: Comparison of isotropic (a) and anisotropic (b) negative parameters. The vertical parameter in (b) has twice the value of the horizontal parameter so its defects favor vertical repulsion. Both images have 2 graylevels and are 64×64 .



(a)

(b)

Figure 7: Comparison of isotropic (a) and anisotropic (b) positive parameters. The vertical parameter in (b) has twice the value of the horizontal parameter. Both images have 7 graylevels and are 64×64 .